Polar-Based OFDM and SC-FDE Links towards Energy-Efficient Gbps Transmission under IM-DD Optical System Constraints [Invited]*

H. Elgala and T.D.C. Little
Department of Electrical and Computer Engineering
Boston University, Boston, Massachusetts
{*helgala, tdcl*}*@bu.edu*

January 1, 2015

MCL Technical Report No. 01-01-2015

Abstract– Recent studies have investigated the use of orthogonal frequency division multiplexing (OFDM) and single carrier frequency-domain equalization (SC-FDE) for Gbps short-range optical wired and wireless access networks based on direct intensity-modulation with direct detection (IM-DD). OFDM systems have the inherent high peak-to-average power ratio (PAPR). SC-FDE systems have lower PAPR, thus outperform comparable OFDM systems in terms of bit-error performance under various practical considerations mainly the limited dynamic-range of operation at the transmitter. In RF-based OFDM and SC-FDE systems, the output signal is bipolar, complex and can not be transmitted in IM-DD systems. Therefore, several power efficient schemes, however spectrally inefficient, have been proposed to make positive OFDM and SC-FDE signals, *e.g.* asymmetrically clipped optical OFDM (ACO-OFDM) and repetition and clipping optical SCFDE (RCO-SCFDE). To increase the data-rate, a novel OFDM and SC-FDE signal formats called polar OFDM (P-OFDM) and polar SC-FDE (P-SC-FDE), based on a polar representation of complex symbols, are proposed. The proposed format offers twice as much spectral efficiency as state-of-the-art unipolar OFDM and SC-FDE formats. Moreover, using a power allocation approach on the time-domain positive samples, the PAPR is further reduced and the numerical evaluation of the bit-error performance under optical source's power and dynamic-range constraints demonstrates superior results towards Gpbs transmission.

*In *Journal of Optical Communications and Networking*, Vol. 7, No, 2, Feb. 2015. This work is supported by the NSF under grant No. EEC-0812056. Any opinions, findings, and recommendations expressed in this material are those of the author(s) and do not necessarily reflect the views of the National Science Foundation.

1 Introduction

The spread of capacity-intensive services, such as interactive 3DTV and mobile cloud services urges the need to provide broadband access network systems. The continuous grow of the data rate demand over the next decades will drive the peak rates per user up to 1Gbps and sustainable data rates of hundreds of Mbps [1]. Furthermore, a higher symmetry between down-link and up-link traffics is expected. Consequently, and to support up to 1Gbps per user wired access, the fiber-to-the-home (FTTH) technology using passive optical network (PON) is becoming a reality in many places all over the world, and offers broadband capacity up to the home's doorstep [2]. Similarly, and to support 1Gbps indoor wireless access, luminaries can be used to transmit data wirelessly based on the visible light communications (VLC) technology while illuminating rooms [3, 4].

The simplest and cost-effective way to modulate the optical carrier is the direct IM-DD. Here, the real-value baseband signal modulates the instantaneous power of the optical carrier (laser diodes (LDs) or light-emitting diodes (LEDs) as optical sources) that is directly detected (photodiodes (PDs) as photo-detectors), *i.e.* the data is transmitted only in intensity domain and there is no frequency or phase domain information. As for low cost sources, the 10-Gbps class directly modulated laser (DML) is a good candidate. In VLC, white light is produced either by mixing the three primary colors (red, green and blue) or through the phosphorus-converted LED (PC-LED) [5, 6].

The widely implemented OFDM is an attractive multi-carrier spectrally-efficient modulation format that offer the simplicity and cost-effectiveness to realize robust Gbps access networks. High data-rates are supported through parallel transmission of high-order multi-level quadrature amplitude modulation (M-QAM) symbols on orthogonal sub-carriers. Further benefits of this modulation scheme include high dispersion and polarization mode dispersion (PMD) tolerance using simple equalization with single-tap equalizers in the frequency domain, adaptive bit and power loading according to the channels frequency response, flexible and dynamic resource allocation through access to sub-carrier granularity and the relatively simple implementation by means of digital signal processing (DSP) techniques. From a networking perspective, OFDM offers a flexible multiple access implementation through orthogonal frequency division multiple access (OFDMA). However, OFDM signals are characterized by high PAPR, thus suffer from non-linear distortions, mainly caused by the limited dynamic-range of optical sources [7]. Another strong candidate is the SC-FDE that utilizes single carrier modulation and frequency domain equalization. SC-FDE has similar performances and essentially the same operations as the OFDM system, but much lower PAPR. SC-FDE technique has been adopted by the 3GPP long term evolution (LTE) standard and its advanced version (LTEA) as uplink multiple access scheme, *i.e.* single carrier frequency division multiplexing access (SC-FDMA). A comparison between the performance of single carrier and multi-carrier modulations is reported in [8]. Recently, several papers reported the introduction of the conventional spectrally-efficient power-inefficient DC-biased optical OFDM (DCO-OFDM) [9], the energy-efficient spectrally-inefficient ACO-OFDM [10] and the energy-efficient spectrally-inefficient low PAPR SC-FDE [11] technologies for short reach optical fiber interconnects and VLC transmission [12].

In optical IM-DD systems, the baseband OFDM and SC-FDE signals must be real-valued and unipolar, *i.e.* positive. However, conventional RF versions of OFDM and SC-FDE signals are complex-valued and bipolar in nature. Therefore, the well-known RF formats has to be modified in order to become suitable for IM-DD systems [13]. A straightforward way is to impose a Hermitian symmetry constraint in the frequency domain on the subcarriers of the inverse fast Fourier

transform (IFFT), *i.e.* the main operation to generate the time-domain OFDM and SC-FDE signals. However, such DCO-OFDM signal generated in the time-domain is still bipolar, *i.e.* DC bias is required for proper operation where the bipolar signal is superimposed on this DC operating point. Significant efforts are devoted to designing optical formats which are purely unipolar for energy-efficient IM-DD systems, *i.e.* DC biasing of the optical source is not require. All well-known solutions that do not require interference estimation and cancelation at the receiver must scarify half the spectral efficiency, *i.e.* the data rates are halved compared to DCO-OFDM. These solutions include the asymmetrically clipped optical OFDM (ACO-OFDM) [14] and the repetition and clipping optical SCFDE (RCO-SCFDE) [15].

To deal with the issues of the loss in spectral efficiency and the signal's vulnerability to nonlinear distortion due to a limited dynamic-range of operation, we propose a novel unipolar version of OFDM and SC-FDE, polar OFDM (P-OFDM) and polar SC-FDE (P-SC-FDE), to offer twice the spectral efficiency compared to the conventional ACO-OFDM and RCO-SCFDE [16]. It is worth mentioning that polar OFDM is investigated in RF, however modulating the RF antenna is fundamentally different from modulating LDs/LEDs in IM-DD systems [17]. The basic idea is that one transmits the amplitude and the phase of the RF complex sample over two consecutive periods. Thus, for the same data-rate, half the amount of bits per sub-carrier is required (low order M-QAM symbols). In addition, and through power allocation in time-domain, the PAPR is inherently reduced to avoid complexity and overhead of PAPR reduction techniques and to support high bit-error ratio (BER) performance under dynamic-range constraint of optical sources. Together with clipping as a conventional approach to reduce the PAPR, the considered power allocation at a fixed average power is similar to power back-off used in RF, however the reduced power from one of the two consecutive periods is allocated to the other period. Throughout the paper, the focus is on the generation of the P-OFDM and the P-SC-FDE signals and presenting the characteristics and performance of the proposed systems in terms of PAPR and BER under fixed power and dynamic-range of operation, *i.e.* the ACO-OFDM system is considered as a benchmark. It is worth pointing out that this work is applicable for direct IM-DD optical fiber as well as optical wireless communications based on either LDs or LEDs.

The remainder of this paper is organized as follows. The conventional energy-efficient ACO-OFDM system is introduced in Section II. In Section III, our proposed polar signal format applied on RF OFDM and SC-FDE to realize a suitable optical versions for IM-DD is highlighted. Optical system constraints are discussed in Section IV. In Section V, the achieved system performance based on simulation results is presented. Conclusions are drawn in Section VI.

2 Energy-efficient ACO-OFDM

The main building blocks of a conventional ACO-OFDM transmission chain is shown in Fig. 1. The data is an input stream of grouped ones and zeros "bit-symbols" based on the considered constellations, *e.g.* M-QAM constellations. The generated complex "QAM-symbols" are then mapped onto the following vector:

$$X_k = \left[\, 0\, X_0 \cdots \; 0 \;\; X_{N/4-1} \;\; 0\, X^*_{N/4-1} \;\; 0 \cdots \;\; X^*_0 \right]^T \tag{1}$$

where, $(.)^*$ denotes the complex conjugate, $(.)^T$ denotes the transpose of a vector and the values $X_k, k = 0, \cdots, N-1$ are the N frequency-domain input symbols. While mapping the QAM-

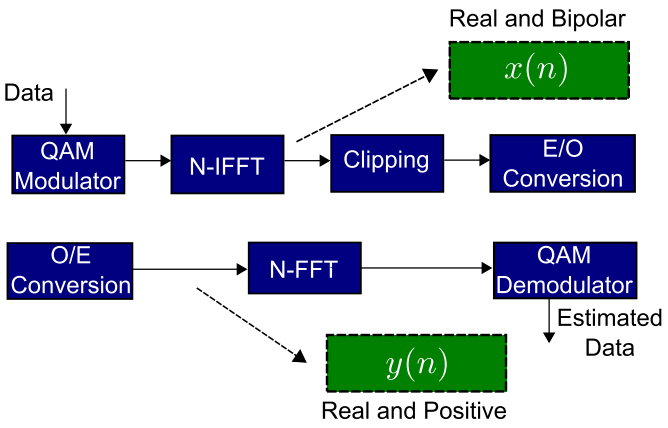

Figure 1: Main building blocks of an ACO-OFDM transmission system.

symbols to only odd indexed subcarriers of the length N IFFT operation, the Hermitian symmetry property of the vector X is needed to insure real-valued output signal. The values of the first and the $N/2$ subcarriers must be also zero to ensure the Hermitian property. The time-domain output signal is generated by taking the IFFT of the vector X_k:

$$x_n = \frac{1}{N} \sum_{k=1}^{N} X_k \exp^{\left(j\frac{2\pi}{N}nk\right)} \tag{2}$$

where, $x_n, n = 0, \cdots, N-1$ are the N time-domain output samples (equivalent to the number of sub-carriers).

Since X_k contains data only on the odd subcarriers, the generated time-domain signal has a half-wave symmetry. The half-wave symmetry means that the same information in the first $N/2$ samples is repeated in the second half of the ACO-OFDM symbol. As a consequence, the negative part can be clipped without any loss of information. This clipping produces a unipolar signal. The intermodulation caused by clipping occurs only in the even indexed subcarriers and does not affect the data-carrying odd indexed subcarriers [14].

Practically, a cyclic prefix (CP) is added to avoid inter-carrier interference (ICI) as well as inter-block interference (IBI) by converting the linear convolution with the channel into a circular one. The resulting unipolar time-domain signal, and after being converted to an analog signal through the digital-to-analog converter (DAC), is used to modulate the intensity of the optical source, *i.e.* electrical-to-optical conversion, E/O.

After the optical-to-electrical conversion, O/E, and CP removal, the received samples of one ACO-OFDM symbol y_n are processed using N-points complex fast Fourier transform (FFT) operation as shown in the following:

$$Y_k = \sum_{n=0}^{N-1} y_n \exp^{\left(-j\frac{2\pi}{N}nk\right)} \tag{3}$$

where, the values $Y_k, k = 0, \cdots, N-1$ are the estimated complex QAM-constellations. Finally, the QAM demodulator is used to estimate the transmitted data symbols.

3 Polar-based OFDM and SC-FDE Formats

3.1 Polar OFDM

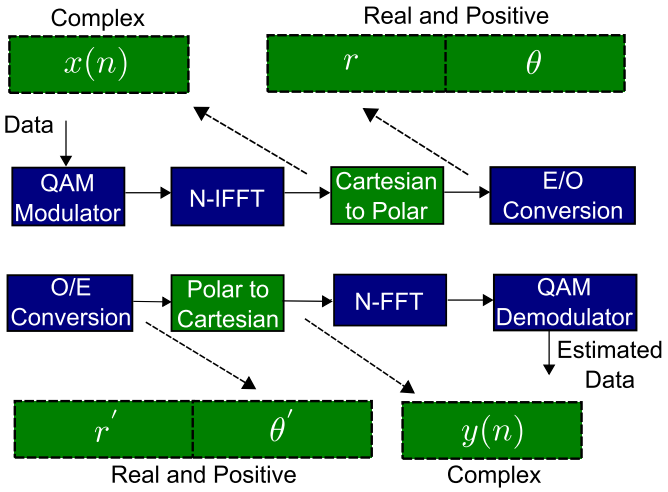

Figure 2: Main building blocks of a P-OFDM transmission system.

As shown in Fig. 2, the P-OFDM signal is obtained based on adding Cartesian-to-Polar and Polar-to-Cartesian operations to conventional RF-OFDM communication chain. The N complex samples forming an OFDM symbol (x_n), after N-points complex IFFT operation, are also described by Equ. (2).

The time-domain output samples x_n are input to the Cartesian-to-Polar operation. The N amplitudes of the different samples ($|x_n| = r_n$) and the N phases of the different samples ($\arg(x_n) = \theta_n$) are transmitted (E/O) (after attaching a CP and applying a DAC) during two consecutive P-OFDM symbol periods of length $2N$. $\theta = 0$ is mapped to value 0 (associated to $I_{\rm L}$) while $\theta = 360^o$ is mapped to value 1 (associated to $I_{\rm H}$), where $I_{\rm L}$ is the minimum drive current (threshold or turn-on current) of the optical source and $I_{\rm H}$ is the maximum allowed drive current. All real-valued signals are constrained by the dynamic-range of the optical source, $\text{DR}_{\text{Source}} = I_{\rm H} - I_{\rm L}$. As a result, the signal is vulnerable to nonlinear baseband distortion, *i.e.* mainly clipping.

After the O/E, the received samples representing the amplitudes of the transmitted samples ($r_n^{'}$) and the phases of the transmitted samples ($\theta_n^{'}$) are used at the input of the Polar-to-Cartesian operation to represent the transmitted complex-valued samples in the polar coordinate system back to the Cartesian coordinate system. The generated N complex samples of one OFDM symbol y_n are processed using N-points complex FFT operation as described by Equ. (3).

3.2 Polar SC-FDE

In P-OFDM, and at the transmitter, an IFFT operation is used to transform the complex "QAM-symbols" from the frequency-domain into time-domain complex signal, *i.e.* samples. The use of an IFFT increases the PAPR of the transmitted signal. However, in P-SC-FDE, after mapping the binary data into complex "QAM-symbols", the real (in-phase) and imaginary (quadrature) parts of the complex symbols are transmitted separately without an IFFT operation.

The time-domain N complex "QAM-symbols" are input to the Cartesian-to-Polar operation. The N-samples r_n and the N-samples θ_n are transmitted (E/O) during two consecutive P-SC-FDE symbol periods of length $2N$. A CP is attached and the signal after the DAC modulates the optical source.

After the O/E, $r_n^{'}$ and $\theta_n^{'}$ are used at the input of the Polar-to-Cartesian operation to represent the transmitted complex-valued samples in the polar coordinate system back to the Cartesian coordinate system. The generated N complex samples of one P-SC-FDE symbol y_n are processed using N-points complex FFT operation followed by FDE before a final IFFT operation as shown in Fig. 3.

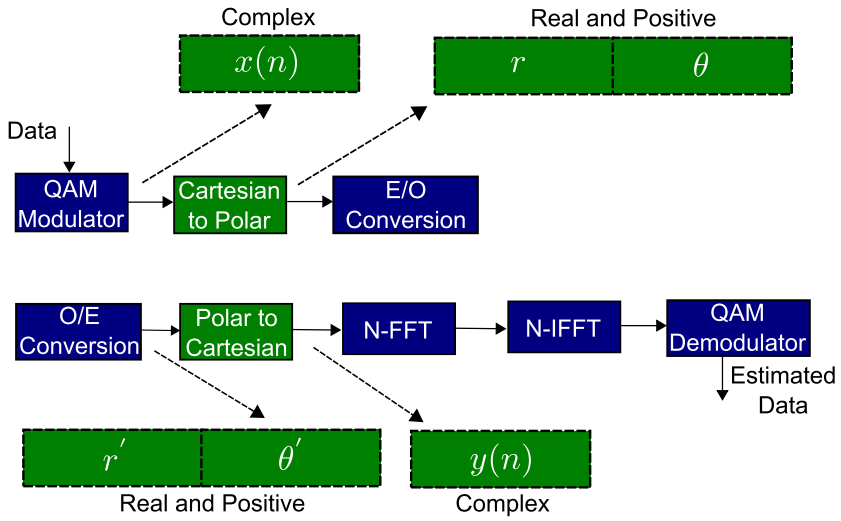

Figure 3: Main building blocks of a P-SC-FDE transmission system.

4 IM-DD System Constraints

4.1 Dynamic-Range of Optical Sources

The IM-DD system is limited by the $\text{DR}_{\text{Source}}$. Each source has a minimum recommended forward current according to the data-sheet, which is the onset of current flow and light emission. Due to thermal aspects, AC/pulsed currents must be limited according to the manufacturer's data-sheet to ensure that the chip does not overheat, in order to avoid E/O efficiency degradation or, in the worst case, total failure. Assuming a predistorter to linearize the input-output characteristic, the output optical power is linear with the drive current, where the limit is determined by I_{L} and I_{H} [18]. Thus, the behavior relating the current through the optical source $i_{\text{Source}}(t)$ to the output optical power $\phi_{\text{Source}}(t)$ can be described as follows:

$$i_{\text{Source}}(t) = \begin{cases} I_{\text{H}} & \text{if } i_{\text{Signal}}(t) \geq I_{\text{H}} \\ i_{\text{Signal}}(t) & \text{if } I_L < i_{\text{Signal}}(t) < I_{\text{H}} \\ I_{\text{L}} & \text{if } i_{\text{Signal}}(t) \leq I_{\text{L}} \end{cases} \tag{4}$$

where, $i_{\text{Signal}}(t)$ is the P-OFDM or P-SC-FDE signal current.

By defining the dynamic-range $i_{\text{Signal}}(t)$ as,

$$\text{DR}_{\text{Signal}} = \max\{x[n]\} - \min\{x[n]\} \tag{5}$$

$\text{DR}_{\text{Signal}}$ is constrained by $\text{DR}_{\text{Source}}$, *i.e.* $\text{DR}_{\text{Signal}} \leq \text{DR}_{\text{Source}}$.

4.2 Average Emitted Power and Peak-to-Average Power Ratio

Since $\phi_{\text{Source}}(t)$ can not be negative, $i_{\text{Source}}(t)$ must be nonnegative, *i.e.* $i_{\text{Source}}(t) > 0$. The contribution of $i_{\text{Signal}}(t)$ to the optical flux $\phi_{\text{Source}}(t)$ is defined as,

$$\phi_{\text{Source}}(t) = \text{E}[i_{\text{Signal}}(t)] \tag{6}$$

where E[.] denotes statistical expectation. Due to the limit on power consumption, eye safety regulation or dimming requirement in case of VLC systems, the system usually operates under some average power constraint defined by P_{Signal}.

In case of ACO-OFDM, the contribution of $i_{\text{Signal}}(t)$ to $\phi_{\text{Source}}(t)$ is set based on a linear scaling such that

$$i_{\text{Signal}}(t) = m \cdot i_{\text{Signal}}(t) \tag{7}$$

where, m is real-valued. The resulting signal has a standard deviation,

$$\sigma_{\text{Signal}} = m \cdot \sqrt{\text{E}[i^2_{\text{Signal}}(t)]} \tag{8}$$

σ_{Signal} can be maximized by selecting a scaling factor with the greatest absolute value. To ensure that $i_{\text{Signal}}(t)$ stays within $\text{DR}_{\text{Source}}$, the greatest value of m is,

$$m = \frac{\text{DR}_{\text{Source}}}{\max\{i_{\text{Signal}}(t)\}} = \frac{I_{\text{H}} - I_{\text{L}}}{\max\{i_{\text{Signal}}(t)\}} \tag{9}$$

In P-OFDM and P-SC-FDE systems, having $k_1|x_n| = k_1 r_n$ and $k_2 \text{arg}(x_n) = k_2\theta_n$, where k_1 and k_2 are scaling factors that control the relative transmit power of the two consecutive periods/parts of the symbol, DR_r is the dynamic-range of the signal representing r_n, *i.e.* $(k_1 r_n)$ and DR_θ is the dynamic range of the signal representing θ_n, *i.e.* $(k_2\theta_n)$. To ensure that DR_r and DR_θ stay within $\text{DR}_{\text{Source}}$, the greatest value of k_1 and k_2 are,

$$k_1 = \frac{\text{DR}_{\text{Source}}}{\max\{r_n\}} = \frac{I_{\text{H}} - I_{\text{L}}}{\max\{r_n\}} \tag{10}$$

$$k_2 = \frac{\text{DR}_{\text{Source}}}{\max\{\theta_n\}} = \frac{I_{\text{H}} - I_{\text{L}}}{\max\{\theta_n\}} \tag{11}$$

Finally, the PAPR is defined as

$$\text{PAPR} = \frac{\max\{x^2[n]\}}{\text{E}[x^2[n]]} \tag{12}$$

5 Results

For Monte Carlo simulations, the system is implemented using 64 FFT/IFFT subcarriers. For a fair comparison between the ACO-OFDM, P-OFDM and P-SC-FDE approaches, (1) the un-coded QAM constellations are set to insure a similar effective data-rate, (2) the average power calculated over one time-domain ACO-OFDM symbol of length N and the two consecutive P-OFDM/P-SC-FDE symbol periods of length $2N$ are maintained equal, *i.e.* $\mathrm{P_{Signal}}$ is maintained constant and (3) the average energy of the constellations is normalized to one, *i.e.* the average energy of x_n is the same as the average energy of the constellations X_k. For Gbps transmission, a high order M-QAM is needed. Consequently, the ACO-OFDM uses 8-bits (256-QAM) while P-OFDM and P-SC-FDE use 4-bits (16-QAM). Using a power allocation approach in the time-domain, $\mathrm{P_{Signal}}$ of the two consecutive P-OFDM/P-SC-FDE symbol periods is split across the r_n and the θ_n periods. Shot noise and thermal noise at the receiver are modeled as additive white Gaussian noise (AWGN) with noise power of -15dBm. A perfect synchronization between the transmitter and the receiver is assumed. A line-of-sight (LOS) configuration is also assumed, thus no samples are considered for CP. The overall channel impulse response including the E/O and O/E conversion are assumed to be non-dispersive with an amplitude of the 1. Using $I_{\mathrm{H}} = 1\mathrm{A}$ and $I_{\mathrm{L}} = I_{\mathrm{th}} = 0\mathrm{A}$, the $k_1 r_n$ and $k_2\theta_n$ sample values beyond $\mathrm{DR_{Source}}$ are clipped at I_{H}.

The influence of $\mathrm{DR_{Source}}$ (quantified by the value of the clipping ratio (CR)) on the BER curves are investigated, where the CR is defined in dB as,

$$\mathrm{CR\ (dB)} = 10\log_{10}\frac{\mathrm{DR_{Source}}}{\mathrm{P_{Signal}}} \tag{13}$$

5.1 Time-domain signals without power allocation

At a fixed $\mathrm{P_{Signal}}$ of 30dBm, and no power allocation, Fig. 4 shows the time-domain samples of the ACO-OFDM using 8-bits (256-QAM), P-OFDM using 4-bits (16-QAM) and P-SC-FDE using 4-bits (16-QAM). One ACO-OFDM symbol consists of $N = 64$ samples. Transmitting a single P-OFDM or P-SC-FDE symbol requires the transmission of $2N = 128$ samples. In ACO-OFDM, the high $\mathrm{DR_{Signal}}$ is obvious relative to that of P-OFDM and P-SC-FDE. In P-OFDM and P-SC-FDE, and regardless of the modulation order, the envelope of the θ_n samples is confined. However, the DR_θ in case of P-OFDM is wider compared to the DR_θ in case of P-SC-FDE. This is clearly demonstrated in Fig. 5, where 16 known time-domain samples are in case of P-SC-FDE while the time-domain samples of P-OFDM have random amplitudes and phases, *i.e.* covering the whole range from $\theta = 0$ up to $\theta = 360^o$. Fig. 5 also confirms the wider dynamic-range of the real-valued time-domain ACO-OFDM samples compared to the complex-valued time-domain (before the Cartesian-to-Polar operation) P-OFDM and P-SC-FDE samples.

5.2 PAPR and BER without power allocation

Using the same system parameters introduced above and again no power allocation (similar to the signals shown in Fig. 4), the cumulative distribution function (CDF) plots of the PAPR for the three signals are depicted in Fig. 6. Indeed P-OFDM offers about 2.5dB reduction compared to ACO-OFDM for the same number of sub-carriers. The PAPR of P-SC-FDE is also about 4.5dB

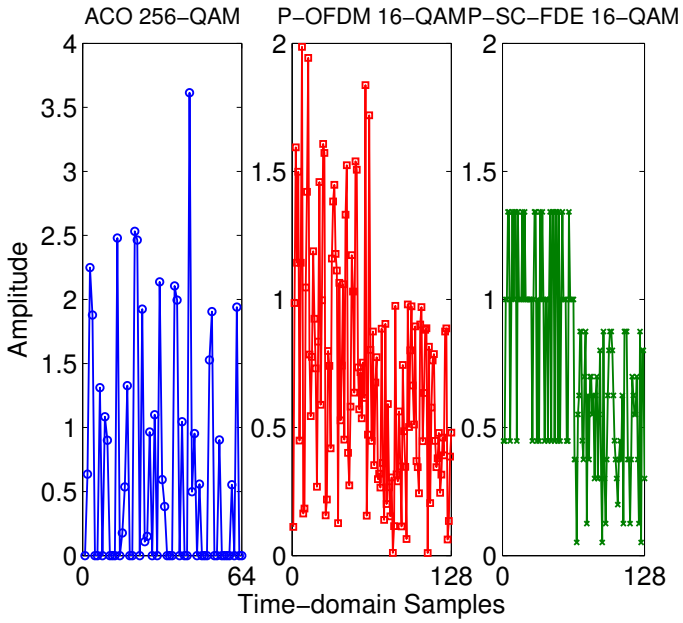

Figure 4: Time-domain ACO-OFDM (left), P-OFDM (middle) and P-SC-FDE (right) samples without power allocation.

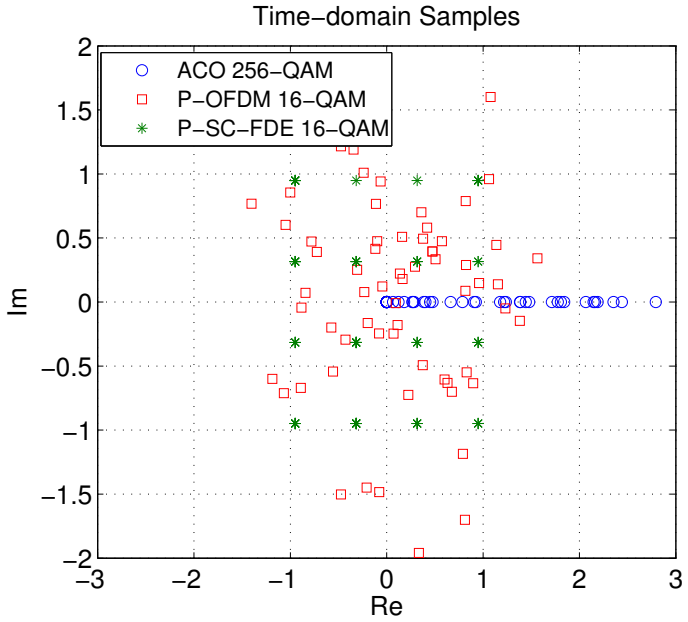

Figure 5: Time-domain ACO-OFDM, P-OFDM and P-SC-FDE samples on a constellation diagram without power allocation.

lower compared to ACO-OFDM and shows a narrower range compared to both PAPR curves of ACO-OFDM and P-OFDM.

The influence of the DR_{Source} on BER curves is also investigated. At a fixed, but reduced, P_{Signal} of 15dBm, it is clearly confirmed that at the same data-rate, P-OFDM and P-SC-FDE offer better

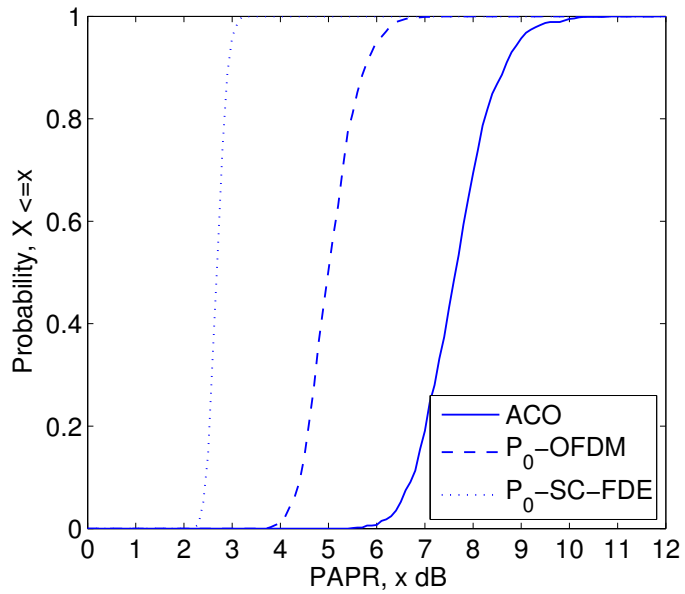

Figure 6: CDF plots of PAPR for $N = 64$ without power allocation.

BER performance compared to ACO-OFDM for CR as low as 2dB (Fig. 7). However, and for the considered parameters, the P-OFDM and P-SC-FDE BER performances do not ensure reliable transmission being above the forward error correction (FEC) limit. The observed BER floor is mainly determined by the considered value of the AWGN. For ACO-OFDM and a target BER of 10^{-3}, CRs below 12dB are not sufficient.

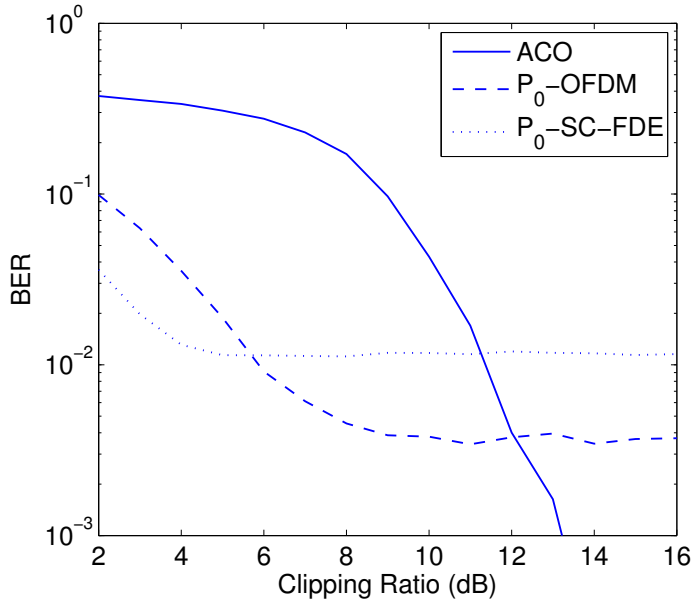

Figure 7: BER vs. CR under dynamic-range constraints without power allocation.

5.3 PAPR and BER with power allocation

Now, we will show how the BER is improved using power allocation in time-domain. At the same fixed P_{Signal} of 15dBm, changing k_1 and k_2 controls the effective PAPR. We investigate the allocation of power in time-domain to the r_n and θ_n periods and show the change of the effective PAPR and the corresponding BER performance at the fixed DR_{Source}. BER curves are obtained for different values of k_1 and k_2, where k_1 is increased relative to k_2. The power allocated to the r_n and θ_n periods in percentage is given in Table 1. At the receiver, the allocated powers are recombined during the regeneration of the complex samples in the Cartesian domain.

Table 1: Power Allocation

	r	θ
P_0	NaN	NaN
P_1	10%	90%
P_2	20%	80%
P_3	30%	70%
P_4	40%	60%
P_5	50%	50%
P_6	60%	40%
P_7	70%	30%
P_8	80%	20%
P_9	90%	10%

In Fig. 8, the CDF plots of the P-OFDM PAPR for the different settings in Table 1 are depicted. Indeed, and relative to P_0 (no power allocation), the PAPR is reduced up to P_4 (Fig. 8 (upper)) and starts increasing beyond P_4 up to P_9 (Fig. 8 (lower)). At P_4 and relative to P_0, and assuming a fixed average power per P-OFDM symbol (amplitude samples period plus phase samples period), the power of phase samples is decreased while the power of amplitude samples is increased (at P_0 high power in phase samples than in amplitude samples, see Fig. 4 (middle)). Giving more power to the amplitude samples increases the P-OFDM symbol average power while reducing the high peaks of the confined dynamic-range phase samples. Moving towards P_9, the power of phase samples is further decreased while the power of amplitude samples is further increased. As the dynamic-range of the amplitude samples is not confined, the probability of high peaks relative to the P-OFDM symbol average is high and accordingly increased PAPR is expected.

The corresponding BER performance of the P-OFDM for the different settings in Table 1 and as a function of the CR is shown in Fig. 9. For P_1, a BER of 10^{-3} at 4dB CR and a BER floor around 3×10^{-5} starting at 5dB CR are achieved. For P_2 and P_3, the BER floor is further improved. Up to P_7 a BER improvement is noticeable compared to P_0 and ACO-OFDM in a CR range between 2dB and 12dB.

In Fig. 10, the CDF plots of the P-SC-FDE PAPR for the different settings in Table 1 are depicted. Relative to P_0 (no power allocation), the PAPR is reduced at P_1 (Fig. 10 (upper)), however increases up to P_6. The PAPR relative to P_6 is decreased at P_7, P_8 and P_9 (Fig. 10 (lower)).

The corresponding BER performance of the P-SC-FDE for the different settings in Table 1 and as a function of the CR is shown in Fig. 11. It is obviously noticed that the BER floor is greatly

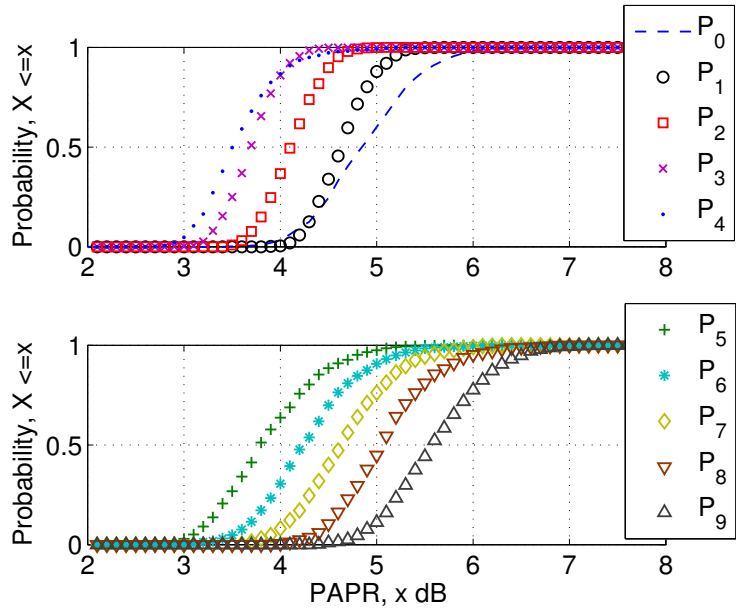

Figure 8: CDF plots of PAPR for P-OFDM using $N = 64$ with power allocation.

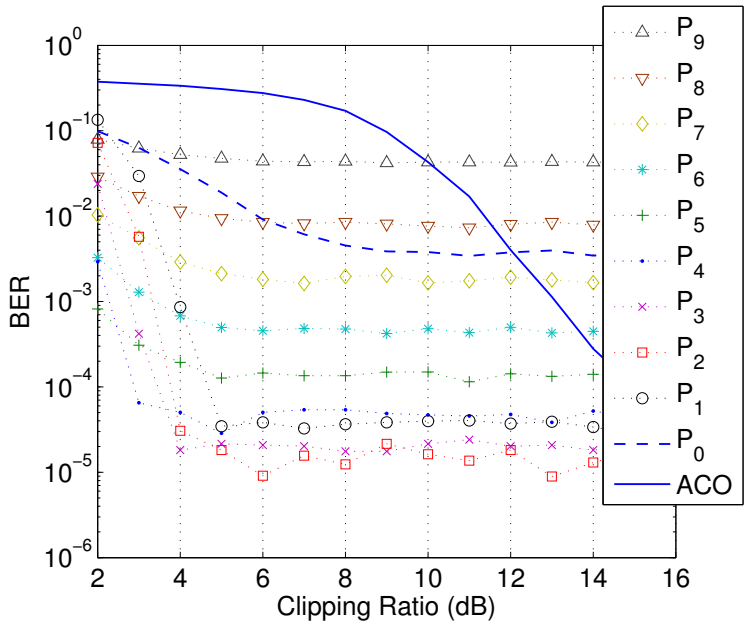

Figure 9: BER vs. CR under dynamic-range constraints for P-OFDM with power allocation.

improved as in the case of P-OFDM. However, the BER is slightly worse compared to P-OFDM. This is related to the wider DR_θ of P-OFDM relative to the DR_θ of P-SC-FDE, making the P-SC-FDE more susceptible to the AWGN (see the signals shown in Fig. 4 and Fig. 5).

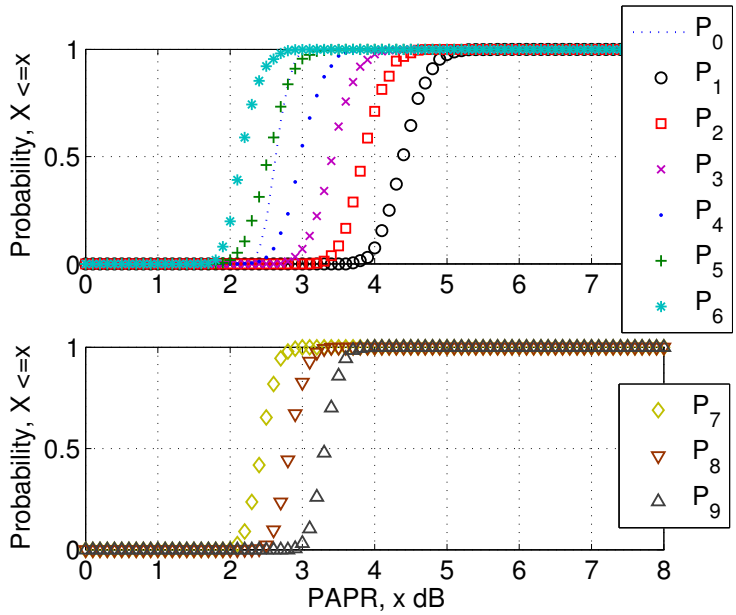

Figure 10: CDF plots of PAPR for P-SC-FDE using $N = 64$ with power allocation.

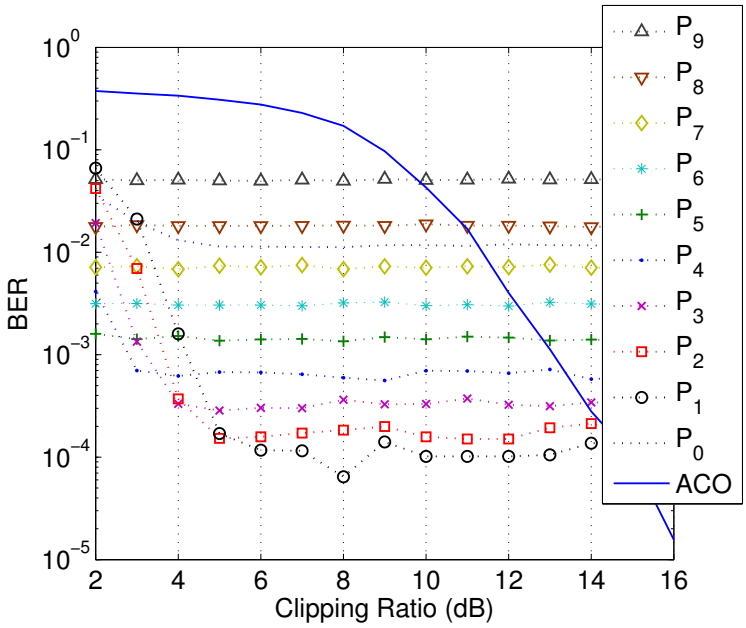

Figure 11: BER vs. CR under dynamic-range constraints for P-SC-FDE with power allocation.

6 Conclusion

The proposed spectrally and energy efficient P-OFDM and P-SC-FDE are analyzed in the context of IM-DD transmission and compared to the well-known energy-efficient ACO-OFDM as a benchmark system. A power allocation approach in time-domain is shown to bring a significant BER performance under narrow dynamic-range of operation as low as 2dB CR at the transmit-

ter. For high order M-QAM, and depending on noise conditions, higher data-rate and better BER performance of P-OFDM and P-SC-FDE compared to ACO-OFDM are feasible under practical conditions of fixed power and dynamic-range of operation.

References

[1] Cisco Visual Networking Index, *Global Mobile Data Traffic Forecast Update, 2012-2017*, White Paper, (CISCO, 2013).

[2] C. Lin, *Broadband Optical Access, FTTH, and Home Networks–the Broadband Future* (Wiley, 2006).

[3] *Visible light communication (VLC) - a potential solution to the global wireless spectrum shortage*, Technical Report, (GBI Research, 2011).

[4] H. Elgala, R. Mesleh, and H. Haas, "Indoor broadcasting via white LEDs and OFDM," *IEEE Transactions on consumer Electronics*, vol. 55, no. 3, pp. 1127–1134, 2009.

[5] J. Gancarz, H. Elgala, and T. D. C. Little, "Impact of lighting requirements on VLC systems," *IEEE Communications Magazine*, vol. 51, no. 12, pp. 34–41, 2013.

[6] H. Elgala, R. Mesleh, and H. Haas, "Indoor Optical Wireless Communication: Potential and State-of-the-Art," *IEEE Communications Magazine*, vol. 49, no. 9, pp. 56–62, 2011.

[7] R. Lin, "Analysis of OFDM signal distortion in optical fiber links," *SPIE Communications and Photonics Conference and Exhibition ACP. Asia*, paper 83091C, pp.1–14, 2011.

[8] J. Li, S. Zhang, F. Zhang and Z. Chen, "Comparison of transmission performances for CO-SCFDE and CO-OFDM systems," *IEEE Photonics Technology Letters*, vol. 22, no. 14, pp. 1054–10562, 2010.

[9] H. Yang, S. C. J. Lee, E. Tangdiongga, F. Breyer, S. Randel, A. M. J. Koonen, "40-Gb/s transmission over 100m graded-index plastic optical fiber based on discrete multitone modulation," *OSA Optical Fiber Communication Conference*, paper PDPD8, 2009.

[10] L. Chen, J. Zhou, Y. Qiao, Z. Huang, Y. Ji, "Novel modulation scheme based on asymmetrically clipped optical orthogonal frequency division multiplexing for next-generation passive optical networks," *IEEE/OSA Journal of Optical Communications and Networking*, vol. 5, no. 8, pp. 881–887, 2013.

[11] V. Teichmann, A. Barreto, T. Pham, R. Rodes, I. Monroy, and D. Mello, "SC-FDE for MMF short reach optical interconnects using directly modulated 850 nm VCSELs," *OSA Optics Express*, vol. 20, no. 23, pp. 25369–25377, 2012.

[12] G. Cossu, A. Khalid, P. Choudhury, R. Corsini, and E. Ciaramella, "3.4 Gbit/s visible optical wireless transmission based on RGB LED," *OSA Optics Express*, vol. 20, no. 26, pp. B501–B506, 2012.

[13] R. Mesleh, H. Elgala, and H. Haas, "On the Performance of Different OFDM Based Optical Wireless Communication Systems," *OSA Journal of Lightwave Technology*, vol. 3, no. 8, pp. 620–628, 2011.

[14] J. Armstrong, and A. J. Lowery, "Power efficient optical OFDM," *IET Electronics Letters*, vol. 42, no. 6, pp. 370–372, 2006.

[15] K. Acolatse, Y. Bar-Ness, and S. K. Wilson, "Novel techniques of single-carrier frequency-domain equalization for optical wireless communications," *EURASIP Journal on Advances in Signal Processing*, vol. 2011, no. 4, 2011.

[16] H. Elgala and T. D. C. Little, "P-OFDM: Spectrally Efficient Unipolar OFDM," *OSA Optical Fiber Communication Conference*, paper Th3G.7, 2014.

[17] M. Talonen and S. Lindfors, "System requirements for OFDM polar transmitter," *IEEE Circuit Theory and Design Conference*, vol. 3, pp. 69–72, 2005.

[18] H. Elgala, R. Mesleh, and H. Haas, "Non-linearity effects and predistortion in optical OFDM wireless transmission using LEDs," *Inderscience Journal of Ultra Wideband Communications and Systems*, vol. 1, no. 2, pp. 143–150, 2009.